

Reconstructing Perceived Images from Brain Activity by Visually-guided Cognitive Representation and Adversarial Learning

Ziqi Ren
Xidian University

Jie Li
Xidian University

Xuetong Xue
Xidian University

Xin Li
UESTC

Fan Yang
UNC

Zhicheng Jiao
UNC

Xinbo Gao
Xidian University

December 21, 2024

Abstract

Reconstructing perceived images based on brain signals measured with functional magnetic resonance imaging (fMRI) is a significant and meaningful task in brain-driven computer vision. However, the inconsistent distribution and representation between fMRI signals and visual images cause the heterogeneity gap, which makes it challenging to learn a reliable mapping between them. Moreover, considering that fMRI signals are extremely high-dimensional and contain a lot of visually-irrelevant information, effectively reducing the noise and encoding powerful visual representations for image reconstruction is also an open problem. We show that it is possible to overcome these challenges by learning a visually-relevant latent representation from fMRI signals guided by the corresponding visual features, and recovering the perceived images via adversarial learning. The resulting framework is called Dual-Variational Autoencoder/Generative Adversarial Network (D-VAE/GAN). By using a novel 3-stage training strategy, it encodes both cognitive and visual features via a dual structure variational autoencoder (D-VAE) to adapt cognitive features to visual feature space, and then learns to reconstruct perceived images with generative adversarial network (GAN). Extensive experiments on three fMRI recording datasets show that D-VAE/GAN achieves more accurate visual reconstruction compared with the state-of-the-art methods.

1 Introduction

Reading human mind has long been an ambitious capability in works of fiction. In recent years, breakthroughs in neuroscience and computer vision have brought such fictional technologies into the realm of science, i.e., brain decoding. Neuroscience studies [23] have suggested that there exist a mapping between visual stimulus and brain activity patterns, which takes a visual stimulus as input and produces the corresponding brain activity patterns. Recent studies [25] find that the mapping is invertible, and the perception is feasible to be reconstructed from brain activity patterns if the inverse mapping is precisely estimated.

Brain decoding can be distinguished into identification, classification and reconstruction. The first two have been recorded promising results [11, 10, 8, 20, 29, 17, 12] while the last one remains unsolved. This is because accurate reconstruction of perceived images requires both high-level semantic knowledge and low-level visual details, it is hard to extract all this information from high-dimensional brain activity signals, such as fMRI. In addition, the domain gap problem remains between cognitive signals and visual features, making the mapping relationship even harder to achieve. Although there have been several attempts at reconstructing the perceived stimuli from brain responses [30, 18, 19, 21, 2], they only produce blurry, cluttered, and low-quality visual images.

Driven by the success of latent models and adversarial learning, we propose a new approach, named Dual-

Variational Autoencoder/ Generative Adversarial Network (D-VAE/GAN), to reconstruct perceived images from fMRI signals. Our key idea is to learn visually important features from high-dimensional and noisy brain signals in a low-dimensional latent space under the guidance of corresponding visual features. More specifically, D-VAE/GAN first generates low-dimensional latent features for both fMRI signals and perceived images with a dual structure variational autoencoder (D-VAE), then learns to capture visually important information and overcome domain gap in this space, and finally decodes the learned cognitive latent features into corresponding visual images. Intuitively, the approach provides two major advantages. First, by learning lower-dimensional latent space for high-dimensional brain signals, the approach is able to filter out most of noise and clutters, and produces a more compressed representation. Second, by adapting cognitive features to visual features in the lower-dimensional latent space, the approach is able to learn visually important features and overcome the domain gap more effectively.

To sum up, our contributions are as follows. 1) We introduce a joint framework, D-VAE/GAN, established by combining the structure of dual VAEs with GAN model to reconstruct perceived images from fMRI. 2) We propose to utilize visual features encoded from viewed stimuli to guide the learning of cognitive latent features from brain signals. Therefore, our approach is able to effectively capture visually important features from high-dimensional fMRI signals and overcome the domain gap. 3) Our D-VAE/GAN is trained with a novel 3-stage training strategy, and achieves significantly more accurate reconstruction results than existing methods on three public fMRI datasets.

2 Related work

Even though research on brain decoding has attracted increasing attention, a relatively limited number of studies focus on perceived image reconstructions to date. Electroencephalography (EEG) [22] and fMRI are two most widely used neural signals in these decoding tasks. EEG has a high temporal resolution but insufficient spatial resolution, and thus is difficult to locate the active regions in the brain. Contrastively, fMRI is capable of providing

more abundant spatial information for higher-precision decoding.

Traditionally, machine learning methods play significant roles in fMRI-based brain decoding tasks. Miyawaki *et al.*, for the first time, proposed spares multinomial logistic regression (SMLR) by using multi-voxel patterns of fMRI signals and multi-scale visual representation to reconstruct the lower-order information such as binary contrast patterns [18]. Schoenmakers *et al.* reconstructed handwritten characters using a straightforward linear Gaussian approach [27]. Fujiwara *et al.* proposed to build a reconstruction model in which image bases can be automatically estimated by Bayesian canonical correlation analysis (BCCA) [4]. However, the linear hypothesis in the proposed model did not conform to the actual visual encoding-decoding process in human brain.

The recent integration of deep learning into neural encoding has been a very successful endeavor [13, 6]. Van Gerven *et al.* reconstructed handwritten digits using deep belief networks [32]. Several proposed deep multi-view representation learning models, such as deep canonically correlated autoencoders (DCCAE) [33] and correlational neural networks (CorrNet) [1], has the ability to learn deep correlational representations, and thus is able to reconstruct each view respectively. However, directly applying the nonlinear maps of DCCAE and CorrNet to limited noisy brain activities is prone to overfitting. A latest neural decoding method is based on multivariate linear regression and deconvolutional neural network (De-CNN) [35]. It is a two-stage cascade model, i.e., it first predicts featuremaps by multivariate linear regression, then reconstruct images by feeding the estimated feature-maps in a pretrained deconvolutional neural network. More recently, Changde Du *et al.* introduced bayesian deep learning to study visual image reconstruction, named a deep generative multiview model (DGMM) [3], which can be viewed as a nonlinear extension of the linear method BCCA. In addition, Yagmur Gltrk *et al.* reconstructed perceived faces with a deep adversarial neural decoding (DAND) model [6], by combining probabilistic inference with deep learning. Furthermore, they trained a deep convolutional generative adversarial network to generate gray scale photos [28]. However, because measured brain signals are usually noisy and contain a lot of redundant information, and more importantly, they are hard to be transferred to visual space

due to the heterogeneity gap, existing deep learning-based brain decoding methods are generally only able to generate blurry and low-accuracy results which are far from satisfaction.

Precise reconstruction of the perceived images essentially requires the model to extract features associating with multiple visual contents (includes color, texture, shape and so on) from brain signals and transmit them to the visual space. Learning a proper representation capturing sufficient visually-relevant features and with less noise for the brain responses then comes a key to reconstruct a high-quality visual image, which is unfortunately ignored by most existing methods. In this work, we propose a joint framework named D-VAE/GAN and a 3-stage training strategy for achieving above goals. On one hand, to build a compact representation for brain signals, we utilize a dual VAE structure to encode both cognitive signals and visual images to lower-dimensional feature spaces. On the other hand, the learned cognitive features are adapted to the visual feature space under the guidance of visual features for bridging the domain gap, and decoded to the corresponding visual image by adversarial learning. These, to the best of our knowledge, have never been done before, and are flexible to extend based on this work.

3 Method

In this section, we first give an overall description about the basic network structures of the encoding model and decoding model. Then, we introduce the proposed framework D-VAE/AGN in detail, and finally we show how to train our D-VAE/GAN with a novel 3-stage training strategy.

3.1 Feature Learning Autoencoder

Our encoding network contains two VAE-based encoder networks. A VAE consists of two networks that encode a data sample x to a latent representation z and decode the latent representation back to data space. The encoder is regularized by imposing a prior over the latent distribution $p(z)$

$$z \sim \text{Enc}(x) = q(z|x), \tilde{x} \sim \text{Dec}(z) = p(x|z), \quad (1)$$

Layers	$Encoder_{\text{Neu}}$	$Encoder_{\text{Vis}}$	G	D
input	x_{cog}	x_{vis}	features	$x_{\text{vis}}/\tilde{x}_{\text{cog}}/\tilde{x}_{\text{vis}}$
layer-1	FC: 1024-D	Conv: (50,50,64)	FC: (13*13*256)	Conv: (50,50,32)
layer-2	δ :128-D ∇ :128-D	Conv: (25,25,128)	Reshape: (13,13,256)	Conv: (25,25,128)
layer-3	\mathbf{z}_{cog} : 128-D	Conv: (13,13,256)	Deconv: (25,25,256)	Conv: (13,13,256)
layer-4		Reshape: (13*13*256)	Deconv: (50,50,128)	Conv: (7,7,256)
layer-5		FC: 1024-D	Deconv: (100,100,32)	Reshape: (7*7*256)
layer-6		δ :128-D ∇ :128-D	$\tilde{\mathbf{x}}_{\text{cog}}/\tilde{\mathbf{x}}_{\text{vis}}$	FC: 256-D
layer-7		\mathbf{z}_{vis} : 128-D		FC: 1-D

Table 1: The details of layer settings in the networks of D-VAE/GAN. The outputs of each network were highlighted.

where \tilde{x} is the output of decoder. Typically, z is modeled with a Gaussian model $N \sim (0, I)$.

The object is to make \tilde{x} similar to x as much as possible, by minimizing the loss:

$$\begin{aligned} L_{\text{VAE}} &= -\mathbb{E}_q(z|x) \left[\log \frac{p(x|z)p(z)}{q(z|x)} \right] \\ &= -\mathbb{E}_q(z|x) [\log p(x|z)] + D_{\text{KL}}(q(z|x) \| p(z)) \\ &= L_{\text{like}}^{\text{pixel}} + L_{\text{prior}}. \end{aligned} \quad (2)$$

In Eq(2), the first term $L_{\text{like}}^{\text{pixel}}$ denotes the reconstruction error, and the second term L_{prior} means the KL divergence [14] between the encoder distribution and a known prior.

3.2 Adversarial Visual Stimuli Generator

In a GAN [5] model, a generator network $\text{Gen}(z)$ maps latent representation z to target data space (image), while a Discriminator network $\text{Dis}(x)$ takes generated and real samples as input and has to make the binary decision whether the input is real or fake. The objective of GAN is to train a best generator that discriminator cannot figure out which one is real data and which one is generated. The solution to this game aims to maximize/minimize the binary cross entropy:

$$L_{\text{GAN}} = \log(\text{Dis}(x)) + \log(1 - \text{Dis}(\text{Gen}(z))), \quad (3)$$

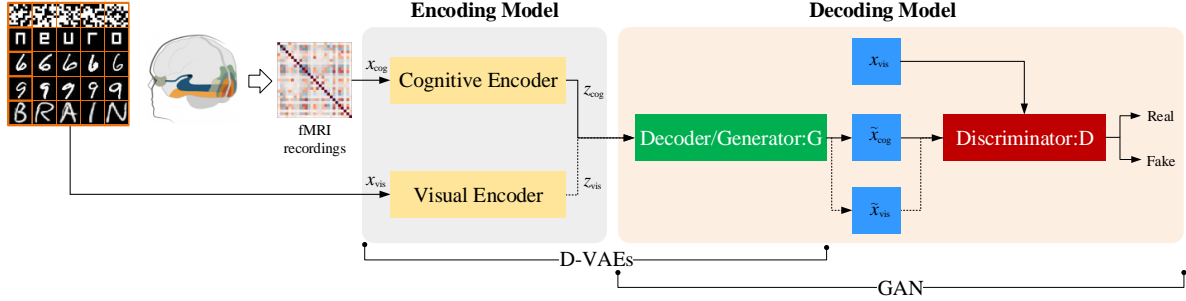


Figure 1: Overview of our D-VAE/GAN, which consists of an encoding model and a decoding model. x_{cog} denotes fMRI data; x_{vis} means stimulus image data; Encoded features of x_{cog} and x_{vis} are gained by Cognitive Encoder and Visual Encoder networks respectively; \tilde{x}_{cog} and \tilde{x}_{vis} are reconstructed images with Generator network (G) based on x_{cog} and x_{vis} respectively; Discriminator (D) and G networks have the same network structure as the basic DCGAN model.

where x is a real sample (stimuli image), z is a vector established from the encoding network and $\text{Gen}(z)$ is a generated image.

In this work, we simply utilize the DCGAN model [24] as our basic GAN structure.

3.3 D-VAE/GAN framework for brain decoding

Overviewed in Fig. 1, the proposed brain decoding framework D-VAE/GAN is composed of two interrelated models: (1) the encoding model specifically designed to have two variational autoencoders: Cognitive Encoder ($\text{Encoder}_{\text{Cog}}$) and Visual Encoder ($\text{Encoder}_{\text{Vis}}$). $\text{Encoder}_{\text{Cog}}$ is used to encode brain response recordings while $\text{Encoder}_{\text{Vis}}$ serves as feature encoder for the corresponding perceived images; (2) the decoding model is formed as a common GAN shared by encoders.

Simply using VAE or GAN individually on brain decoding are usually unreliable. On one hand, the collapse problem of GAN makes it difficult to be applied to brain decoding directly [26]. On the other hand, element-wise reconstruction errors of traditional VAEs may cause generated images blurry [15]. Therefore, in our framework, the two models are combined and trained synchronously, with the generator of GAN also being the decoder of VAEs. Through above combination, the GAN-based de-

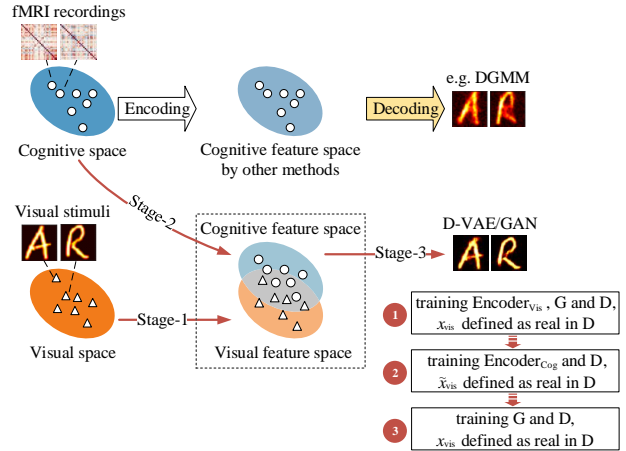


Figure 2: The process of mapping fMRI recordings from cognitive space to visual images. Our method with the 3-stage strategy is in ‘red’, other methods (e.g DGMM) are in ‘white’ and ‘yellow’. The gray dotted box means a hybrid latent feature space.

coding model can be constrained by VAEs, so as to produce more reasonable reconstruction results. Moreover, we take advantage of the appealing property of the discriminator network in GAN, which implicitly has to learn a rich similarity metric for images so as to discriminate

them from “non-images”. We also propose to replace one part of the VAE reconstruction error term $L_{\text{like}}^{\text{pixel}}$ with a reconstruction error $L_{\text{like}}^{\text{Dis}_l}$ expressed in the GAN discriminator, where $\text{Dis}_l(x)$ denotes the l -th layer of D net, to supervise optimization of the reconstruction framework with feature-wise errors.

By taking advantage of VAE and GAN, the various components in D-VAE/GAN are designed capable to well assist each other to achieve overall co-optimization. After jointly training, the learned reconstruction framework will be a structure composed of an effective encoding model of mapping fMRI data into a visually-related latent space z , and a high-quality generation model which decoding the latent feature representations accurately back to visual space.

For all our experiments, we use convolutional and deconvolution architectures with stride=2 to upscale images in Decoder/Generator. Deconvolution is achieved by flipping the convolution direction such that striding causes upsampling. The Cognitive Encoder and Visual Encoder take as input vectors of n -dimensional fMRI recordings and visual stimuli respectively. Discriminator takes as input images of Decoder/Generator’s output and real visual stimuli. Such inputs then go through all layers with 5×5 kernel size. The details of layer settings in the networks of our framework are presented in Table 1.

Training procedure of the framework can be divided into three stages, as illustrated in Fig. 2. The details are as follows.

Optimization of Visual Encoder: In the first stage, the original images are used as input to train $Encoder_{\text{vis}}$ network and decoding model. The $Encoder_{\text{vis}}$ is optimized to encode a stimuli image sample x_{vis} to an appropriate latent visual representation z_{vis} . The Generator/Decoder(G) network is trained to decode z_{vis} accurately back to x_{vis} :

$$\begin{aligned} z_{\text{vis}} &\sim \text{Enc}_{\text{vis}}(x_{\text{vis}}) = q(z_{\text{vis}} | x_{\text{vis}}) \\ \tilde{x}_{\text{vis}} &\sim \text{Gen}(z_{\text{vis}}) = p(x_{\text{vis}} | z_{\text{vis}}), \end{aligned} \quad (4)$$

where $\tilde{x}_{\text{vis}} \sim \text{Gen}(z_{\text{vis}})$ is the sample from G of x_{vis} , and the L_{prior} becomes:

$$L_{\text{prior,VE-opt.}} = D_{\text{KL}}(q(z_{\text{vis}} | x_{\text{vis}}) \| p(z_{\text{vis}})). \quad (5)$$

In addition, the GAN loss in stage-1 is defined as:

$$L_{\text{GAN,VE-opt.}} = \log(\text{Dis}(x_{\text{vis}})) + \log(1 - \text{Dis}(\text{Gen}(z_{\text{vis}}))). \quad (6)$$

We introduce a Gaussian observation model for $\text{Dis}_l(x)$ with mean $\text{Dis}_l(\tilde{x})$ and identity covariance:

$$p(\text{Dis}(x_{\text{vis}} | z_{\text{vis}})) = N(\text{Dis}_l(x_{\text{vis}}) | \text{Dis}_l(\tilde{x}_{\text{vis}}), \mathbf{I}). \quad (7)$$

We can now replace the VAE error of Eq(2) with

$$L_{\text{like,VE-opt.}}^{\text{Dis}_l} = -E_q(z_{\text{vis}} | x_{\text{vis}}) [\log p(\text{Dis}_l(x_{\text{vis}}) | z_{\text{vis}})]. \quad (8)$$

Finally, we train our joint framework in stage-1 with a triple criterion:

$$L = L_{\text{prior,VE-opt.}} + L_{\text{like,VE-opt.}}^{\text{Dis}_l} + L_{\text{GAN,VE-opt.}}. \quad (9)$$

Optimization of Visually-guided Cognitive Encoder:

In the second stage, fMRI data are used as input to train $Encoder_{\text{cog}}$ and decoding model with G fixed. The $Encoder_{\text{cog}}$ is optimized to encode a fMRI sample x_{cog} to a latent cognitive representation z_{cog} close to the related z_{vis} as much as possible. Then G decodes z_{cog} back to visual space:

$$z_{\text{cog}} \sim \text{Enc}_{\text{cog}}(x_{\text{cog}}) = q(z_{\text{cog}} | x_{\text{cog}}), \quad (10)$$

and the L_{prior} becomes:

$$L_{\text{prior,CE-opt.}} = D_{\text{KL}}(q(z_{\text{cog}} | x_{\text{cog}}) \| p(z_{\text{cog}})). \quad (11)$$

Specifically, we define \tilde{x}_{vis} as real to Discriminator(D) for the optimization of $Encoder_{\text{cog}}$ and z_{cog} . So the distribution of G is modeled as:

$$\tilde{x}_{\text{cog}} \sim \text{Gen}(z_{\text{cog}}) = p(\tilde{x}_{\text{vis}} | z_{\text{cog}}), \quad (12)$$

where $\tilde{x}_{\text{cog}} \sim \text{Gen}(z_{\text{cog}})$ is the sample from G of x_{cog} , and the GAN loss is replaced as:

$$L_{\text{GAN,CE-opt.}} = \log(\text{Dis}(\tilde{x}_{\text{vis}})) + \log(1 - \text{Dis}(\text{Gen}(z_{\text{cog}}))). \quad (13)$$

Then the $\text{Dis}_l(x)$ is defined as:

$$p(\text{Dis}(\tilde{x}_{\text{vis}} | z_{\text{cog}})) = N(\text{Dis}_l(\tilde{x}_{\text{vis}}) | \text{Dis}_l(\tilde{x}_{\text{cog}}), \mathbf{I}). \quad (14)$$

We now define the $L_{\text{like}}^{\text{Dis}_l}$ as:

$$L_{\text{like_CE-opt.}}^{\text{Dis}_l} = -\mathbb{E}_q(z_{\text{cog}} | \tilde{x}_{\text{vis}}) [\log p(\text{Dis}_l(\tilde{x}_{\text{vis}}) | z_{\text{cog}})]. \quad (15)$$

Finally, we train the joint framework in step-2 with the triple criterion:

$$L = L_{\text{prior_CE-opt.}} + L_{\text{like_CE-opt.}}^{\text{Dis}_l} + L_{\text{GAN_CE-opt.}}. \quad (16)$$

Specifically, the instances and their encoded features in both cognitive and visual space after stage-2 are illustrated in Fig. 3, which shows that two “feature spaces” are closer after feature learning. In another word, the distribution of learned cognitive features is quite similar to that of corresponding visual features directly extracted from viewed images, which contain sufficient visually-relevant information with less noise.

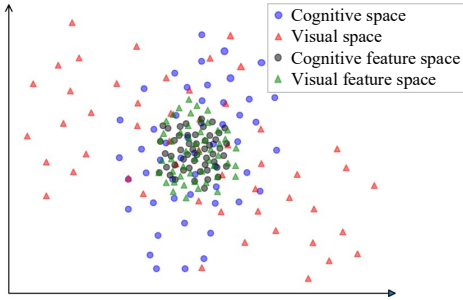


Figure 3: We use t-SNE[16] for dimensionality reduction and visualization of data spaces. Two “feature spaces” are closer after stage-2.

Optimization of Visual Stimuli Generator: In the third stage, we train the framework on the basis of stage-2 with G unfixed and $Encoder_{\text{Cog}}$ fixed to further optimize G . Different from stage-2, we reuse x_{vis} as real to D . Thus, G is optimized to a state that more appropriate to map the learned cognitive representation z_{cog} , instead of the visual representation z_{vis} , back to visual space:

$$\tilde{x}_{\text{cog}} \sim \text{Gen}(z_{\text{cog}}) = p(x_{\text{vis}} | z_{\text{cog}}). \quad (17)$$

Then the GAN loss becomes:

$$L_{\text{GAN_G-opt.}} = \log(\text{Dis}(x_{\text{vis}})) + \log(1 - \text{Dis}(\text{Gen}(z_{\text{cog}}))). \quad (18)$$

Dataset	Instances	Pixels	Voxels	ROIs	Training
Dataset1	2040	100	5438	V1	1320
Dataset2	100	784	3092	V1,V2,V3	90
Dataset3	360	3136	2420	V1,V2	330

Table 2: The details of the 3 datasets used in our experiments. ROIs indicate the related visual regions of interest in brain.

Thus, we train the framework in stage-3 with the criterion:

$$L = L_{\text{GAN_G-opt.}}. \quad (19)$$

4 Experiments

We evaluate our method for perceived image reconstruction on three widely used visual-related fMRI decoding datasets [18, 32, 27]. We operate rigorous experiments and compare with several representative methods, especially with the state-of-the-art method DGMM.

4.1 Datasets

Dataset1 [18], consisting of contrast-defined 10×10 patches, contains two independent sessions. One is a ‘random image session’, in which spatially random patterns were sequentially presented. The other is a ‘figure image session’, in which alphabetical letters and simple geometric shapes were sequentially presented. We used fMRI data from primary visual area V1 of subject 1 (S1) for the analysis. Note that all compared algorithms were trained on the data from ‘random image session’ and evaluated on the data from ‘figure image session’, according to corresponding literature.

Dataset2 [32] contains a hundred handwritten gray-scale digits (equal number of 6s and 9s) at a 28×28 pixel resolution taken from the training set of the MNIST database and the fMRI data from V1, V2, and V3.

Dataset3 [27] contains 360 gray-scale handwritten characters (equal number of Bs, Rs, As, Is, Ns, and Ss) at a 56×56 pixel resolution taken from [31] and the fMRI data of V1, V2 taken from three subjects.

The details of the three datasets used in our experiments are summarized in Table 2. Note that compared with existing methods, we did not perform voxel selection on the

presented fMRI data in preprocessing, which has been included in our encoding model.

In the training section, we resize the input of image data to 100×100 to make the framework convenient for direct application on all three datasets without redundant adjustment of network parameters. Correspondingly, we set a down-sampling operation after reconstruction in post-processing.

Our method is implemented with Python and Tensorflow. We use Adam with $\beta=0.9$. The base learning rate is 3×10^{-4} , and we use exponential_decay (Tensorflow function) with decay_rate=0.98 to lower the learning rate as the training process. Training and testing are performed on an Nvidia 1080Ti GPU with 11G RAM. The ratio of Generator to Discriminator during training section in stage-3 is set as 3:2.

4.2 Reconstruction results

In this section, we present the reconstructed geometric shapes and alphabet letters, handwritten digits, and handwritten characters by the D-VAE/GAN framework and other methods. As shown in Fig. 4, Fig. 5, and Fig. 6 respectively, the first rows denote presented stimulus images, and below rows are the reconstructed images obtained from all compared algorithms.

Qualitative Results: Overall, the images reconstructed by D-VAE/GAN capture the essential features of the presented images. In particular, they show fine reconstructions for handwritten digits and characters. Compared with other algorithms, there is a considerable improvement of image details on the definition of stroke characteristics and the similarity of shape characteristics for Dataset2 and Dataset3. Although the reconstructed geometric shapes and alphabet letters of Dataset1 have some noise in the peripheral regions, the main shapes can be distinguished more clearly than other compared algorithms. Especially, the reconstruction of alphabetical letters (the five images on the right side of the bottom row in Fig. 4) is greatly improved. In general, the reconstructed images by our method possess almost exactly the same shape characteristics as their corresponding original images.

Quantitative Results: To evaluate the reconstruction performance quantitatively, we used several standard image similarity metrics, including Pearson’s correlation coef-

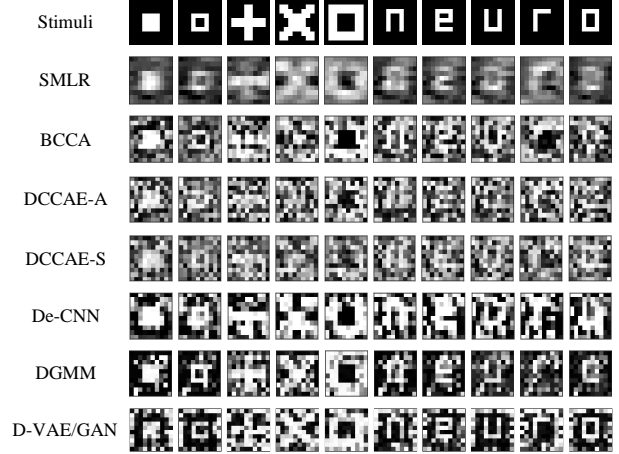


Figure 4: Reconstructions of geometric shapes and alphabet letters taken from Dataset1.

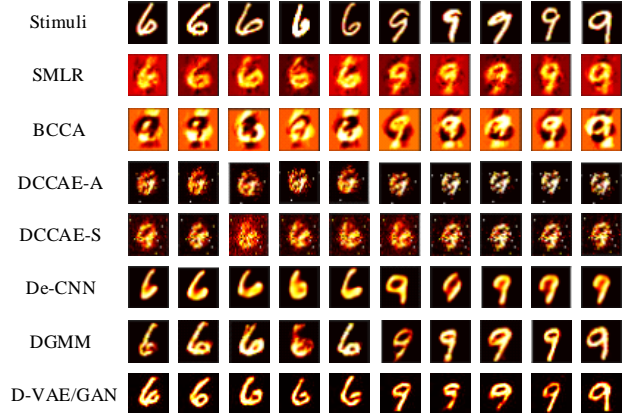


Figure 5: Reconstructions of 10 distinct handwritten digits taken from Dataset2.

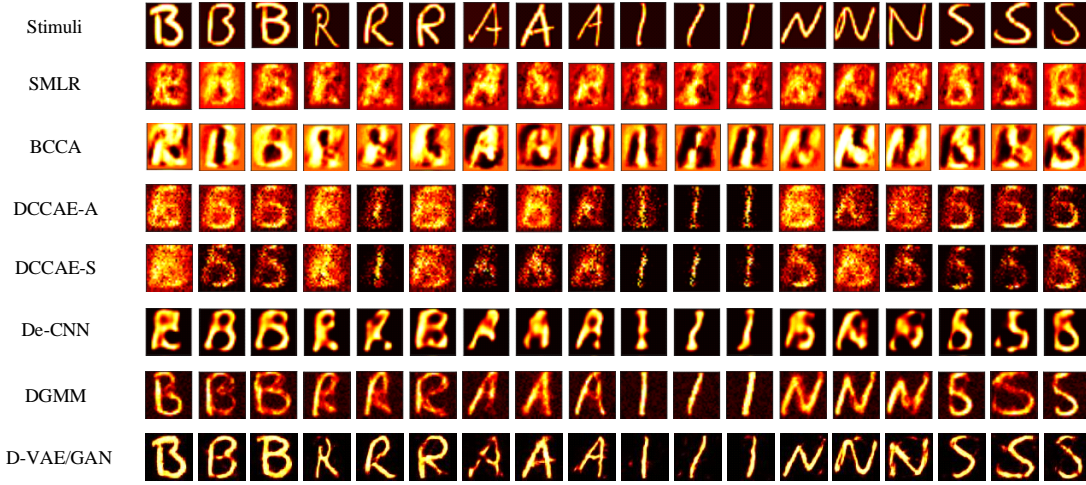


Figure 6: Reconstructions of 18 distinct handwritten characters taken from Dataset3.

Datasets	Algorithms	PCC	MSE	SSIM	ACC-SVM
Dataset1	SMLR	.609 \pm .151	.162 \pm .025	.237 \pm .105	-
	BCCA	.438 \pm .215	.253 \pm .051	.181 \pm .066	-
	DCCAE-A	.455 \pm .113	.234 \pm .029	.166 \pm .025	-
	DCCAE-S	.401 \pm .100	.240 \pm .027	.175 \pm .011	-
	De-CNN	.469 \pm .149	.263 \pm .067	.224 \pm .129	-
	DGMM	.611 \pm .183	.159\pm.112	.268 \pm .106	-
	D-VAE/GAN	.647\pm.001	.250 \pm .006	.283\pm.010	-
Dataset2	SMLR	.767 \pm .033	.042 \pm .007	.466 \pm .030	1.00
	BCCA	.411 \pm .157	.119 \pm .017	.192 \pm .035	1.00
	DCCAE-A	.548 \pm .044	.074 \pm .010	.358 \pm .097	.900
	DCCAE-S	.511 \pm .057	.080 \pm .016	.552 \pm .088	1.00
	De-CNN	.799 \pm .062	.038 \pm .010	.613 \pm .043	1.00
	DGMM	.803 \pm .063	.037 \pm .014	.645 \pm .054	1.00
	D-VAE/GAN	.837\pm.014	.030\pm.002	.714\pm.014	1.00
Dataset3	SMLR	.481 \pm .096	.067 \pm .026	.191 \pm .043	.655 \pm .193
	BCCA	.348 \pm .138	.128 \pm .049	.058 \pm .042	.633 \pm .034
	DCCAE-A	.354 \pm .167	.073 \pm .036	.186 \pm .234	.478 \pm .126
	DCCAE-S	.351 \pm .153	.086 \pm .031	.179 \pm .117	.478 \pm .051
	De-CNN	.470 \pm .149	.084 \pm .035	.322 \pm .118	.589 \pm .135
	DGMM	.498 \pm .193	.058 \pm .031	.340 \pm .051	.767 \pm .115
	D-VAE/GAN	.740\pm.020	.041\pm.003	.587\pm.019	.870\pm.004

Table 3: Performance of several image reconstruction methods on the test datasets. Results were averaged over 20 random seeds and all subjects (mean \pm std). The best performance on each dataset was highlighted.

ficient (PCC), mean squared error (MSE), and structural similarity index (SSIM) [34]. Note that MSE is not highly indicative of perceived similarity, while SSIM can address this shortcoming by taking texture into account.

In addition, we also performed image classification analysis to quantify the reconstruction accuracy from another perspective. Specifically, linear support vector machines (SVMs) trained on the presented visual images were used as the classifiers to label the reconstructed images. Performance comparisons are listed in Table 3. Several observations can be drawn as follows.

Firstly, we can find that the proposed D-VAE/GAN performs considerably above other methods in all indicators on Dataset2 and Dataset3, especially a great promotion on Dataset3. Also, there is a significant improvement in PCC and SSIM on Dataset1. Notably, it is known that a small translation might result in a large pixel-wise error (such as MSE), whereas a human would barely notice the change if the main information of image (shape, object et al) can be well-recognized. Therefore, the SSIM index, which is more consistent with the properties of human vision system (HV-S), indicates that our reconstructed results are better.

Secondly, correct classifications of most compared algorithms are 100% on Dataset2. We believe that it is caused by the fact that digit 6 and 9 are easy to distinguish

from each other. On Dataset3, the prominently higher classification performance on the images reconstructed by our framework demonstrates the superiority of the proposed method.

Finally, it is noteworthy that standard deviations in all indicators of reconstructed images by D-VAE/GAN on all three datasets are quite smaller than that by other compared methods. This implies that our method performs considerably stable reconstruction capability on all presented fMRI data. In another word, it has demonstrated strong robustness and encouraging generalization.

4.3 Comparisons about framework structure

In order to further validate the superiority of the proposed D-VAE/GAN framework, we performed a series of control experiments as follows.

Standard DCGAN: We have attempted to implement reconstruction experiments just by a standard DCGAN structure, i.e. without the encoding model. The parameter settings in DCGAN are same as those in the decoding model of original D-VAE/GAN framework.

The DCGAN models were non-convergent on Dataset1 and Dataset3 (thus we did not show their results here). And though it was convergent on Dataset2, the reconstruction accuracy is quite dissatisfactory (as shown in Fig. 7 and Table 4), even the reconstructed ‘6’s and ‘9’s are confusing. Thus, simply using GAN individually on brain decoding but without encoding the brain responses is somewhat unreliable.

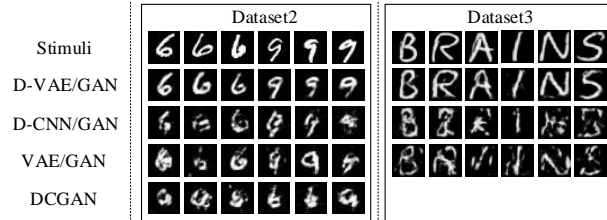


Figure 7: Reconstructions by contrast structures on Dataset2 and Dataset3. The DCGAN model was non-convergent on Dataset3, thus its reconstructed results were not presented here.

Datasets	Structures	PCC	MSE	SSIM	ACC-SVM
Dataset1	DCGAN	$-.123 \pm .008$	$.451 \pm .003$	$-.006 \pm .006$	-
	VAE/GAN	$.002 \pm .009$	$.402 \pm .004$	$.007 \pm .005$	-
	D-CNN/GAN	$.073 \pm .004$	$.483 \pm .005$	$.071 \pm .005$	-
	D-VAE/GAN	$.647 \pm .001$	$.250 \pm .006$	$.283 \pm .010$	-
Dataset2	DCGAN	$.492 \pm .030$	$.083 \pm .005$	$.400 \pm .016$	$.370 \pm .021$
	VAE/GAN	$.534 \pm .043$	$.076 \pm .006$	$.414 \pm .017$	$.490 \pm .030$
	D-CNN/GAN	$.481 \pm .038$	$.088 \pm .008$	$.430 \pm .023$	$.480 \pm .300$
	D-VAE/GAN	$.837 \pm .014$	$.030 \pm .002$	$.714 \pm .014$	1.00
Dataset3	DCGAN	$.023 \pm .003$	$.425 \pm .004$	$.002 \pm .001$	$.203 \pm .007$
	VAE/GAN	$.152 \pm .026$	$.124 \pm .005$	$.277 \pm .010$	$.180 \pm .004$
	D-CNN/GAN	$.136 \pm .022$	$.123 \pm .006$	$.300 \pm .017$	$.120 \pm .005$
	D-VAE/GAN	$.740 \pm .020$	$.041 \pm .003$	$.587 \pm .019$	$.870 \pm .004$

Table 4: Reconstruction performance of contrast structures in Dataset1, Dataset2 and Dataset3. The best performance on each dataset was highlighted.

VAE/GAN: In order to validate the contribution of the guidance by visual features to the cognitive feature learning of fMRI signals, we took away the Visual Encoder network from D-VAE/GAN and conducted contrast experiments. The simplified structure is called VAE/GAN here, whose parameter settings are corresponding to D-VAE/GAN.

As shown in Fig. 7, on Dataset2 and Dataset3, VAE/GAN achieves quite worse reconstruction than D-VAE/GAN which contains Visual Encoder. Besides, vast majority of reconstructed images by VAE/GAN in Dataset1 almost completely cannot be identified (thus we did not show them here). And the quantitative evaluation results by VAE/GAN are also quite worse, as presented in Table 4. In another word, it leads to better brain decoding indeed by visually-guided cognitive features.

D-CNN/GAN: To further investigate the superiority of using VAE for feature learning in our framework, we performed a control experiment by using standard Convolutional Neural Networks (CNNs) to replace VAEs in the encoding model with same parameter settings (the changed structure called D-CNN/GAN here).

As shown in Fig. 7, the reconstructed images by D-CNN/GAN in Dataset2 and Dataset3 are quite worse than those by our original VAE-based framework D-VAE/GAN. Moreover, most reconstructed images by D-CNN/GAN in Dataset1 also almost completely cannot be identified (thus we did not show them here). Correspondingly, the quantitative evaluation results (presented in Table 4) with CNNs encoding are quite dissatisfactory. In

contrast, the application of VAE helps the joint framework achieve more accurate reconstruction results.

4.4 Reconstruction performance in different ROIs

Human visual computing is a very complex process across hierarchical visual function areas (V1 to V5, etc.) on the cerebral cortex. In this section, we explore the contributions of the fMRI data separately taken from different ROIs to perceived image reconstruction. Experiments were implemented on Dataset3 (separate fMRI data from different ROIs are unavailable in Dataset1 and Dataset2) to evaluate the performance of V1/V2 from three subjects. Numbers of voxels, reconstructed images and quantitative evaluations of per ROI are presented in Table 5 and Fig. 8.

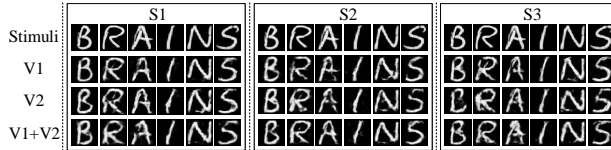


Figure 8: Reconstructions in different ROIs (V1, V2 and V1+V2 included) on Dataset3.

Subjects	ROI	Voxels	PCC	MSE	SSIM	ACC-SVM
S1	V1	948	.740±.017	.040±.003	.601±.021	.840±.003
	V2	1588	.745±.018	.042±.004	.575±.022	.900±.003
	V1+V2	2536	.737±.020	.041±.003	.566±.021	.825±.009
S2	V1	1223	.740±.021	.040±.003	.603±.021	.835±.005
	V2	1561	.743±.020	.041±.003	.554±.021	.863±.005
	V1+V2	2784	.745±.018	.040±.003	.614±.020	.818±.007
S3	V1	1209	.745±.020	.040±.003	.552±.019	.840±.005
	V2	1211	.668±.025	.050±.004	.579±.025	.828±.008
	V1+V2	2420	.740±.020	.041±.003	.587±.019	.870±.004

Table 5: Performance in different ROIs on Dataset3. The best performance on each subject was highlighted.

As shown in Table 5, the lower-level visual ROI V1 performs more stable capability to a certain degree than the higher-level visual ROI V2 or the combined ROIs V1+V2 on most subjects (S1, S2). In Fig. 8, most reconstructed images of V1 performs better quality than V2, especially for more complex characters ‘B’, ‘R’, ‘A’ and ‘N’ (some

blurred pixels and redundant strokes existing in the results of V2). In addition, contrasting the reconstructed results of V1 and V1+V2, we find no obvious superiority when utilizing the fMRI data from both ROIs at the same time by direct combination. It shows that the choice of ROIs can affect decoding performance. Thus for simple visual stimuli, it is analyzed that a majority of utilized visual features are low-level features, which tend to be better reconstructed from fMRI signals in lower rather than higher-level ROIs [9].

In addition, the combination of different ROIs has an intricacy mechanism [7]. In this paper, we combine the fMRI data obtained from V1 and V2 directly to perform reconstruction, as a simple simulation of this ROI combination mechanism in brain. On this basis, we believe that making more efforts to explore more brain-like ROI combination mechanisms can further promote the study of brain decoding.

5 Conclusions and future work

Although the application of reconstructing visual experience from brain responses in an actual context may still be something which humanity will not be able to achieve for a while, an approximately accurate visual reconstruction of artificial visual stimuli has already been achieved successfully in this work. We propose to improve the reconstruction accuracy by encoding the noisy and high-dimensional brain signals to a compact visually-relevant cognitive representation under the guidance of corresponding visual features extracted from stimulus images. On this basis, we propose a novel joint framework D-VAE/GAN and a 3-stage training strategy to tackle this reconstruction task. We take advantage of the encoding ability of VAE to encode fMRI signals and visual images, and then recover the stimulus images through adversarial learning. It is noteworthy that we achieve the visual reconstruction corresponding to each original image but not just of several image categories. For the handwritten digits and handwritten characters, the shape differences among the reconstructed images in same category can be clearly distinguished, which comes a promising result for exploring a totally accurate mind reading in the future. Of course, improvements can be made: the encoder networks used in our framework can be flexibly replaced if

other similar networks could perform better, or for other generation tasks if necessary.

As future work, we plan a) to apply these visual and cognitive features to further interdisciplinary studies of neuroscience, computer vision, and brain-computer interaction; b) to see if more appropriate combination of different visual ROIs in human brain would further improve the decoding performance.

References

- [1] S. Chandar, M. M. Khapra, H. Larochelle, and B. Ravindran. Correlational neural networks. *Neural computation*, 28(2):257–285, 2016. 2
- [2] A. S. Cowen, M. M. Chun, and B. A. Kuhl. Neural portraits of perception: reconstructing face images from evoked brain activity. *Neuroimage*, 94:12–22, 2014. 1
- [3] C. Du, C. Du, and H. He. Sharing deep generative representation for perceived image reconstruction from human brain activity. *arXiv preprint arXiv:1704.07575*, 2017. 2
- [4] Y. Fujiwara, Y. Miyawaki, and Y. Kamitani. Modular encoding and decoding models derived from bayesian canonical correlation analysis. *Neural computation*, 25(4):979–1005, 2013. 2
- [5] I. Goodfellow, J. Pouget-Abadie, M. Mirza, B. Xu, D. Warde-Farley, S. Ozair, A. Courville, and Y. Bengio. Generative adversarial nets. In *Advances in neural information processing systems*, pages 2672–2680, 2014. 3
- [6] Y. Güçlütürk, U. Güçlü, K. Seeliger, S. Bosch, R. van Lier, and M. A. van Gerven. Reconstructing perceived faces from brain activations with deep adversarial neural decoding. In *Advances in Neural Information Processing Systems*, pages 4246–4257, 2017. 2
- [7] U. Hasson, I. Levy, M. Behrmann, T. Hendler, and R. Malach. Eccentricity bias as an organizing principle for human high-order object areas. *Neuron*, 34(3):479–490, 2002. 10
- [8] J. V. Haxby, M. I. Gobbini, M. L. Furey, A. Ishai, J. L. Schouten, and P. Pietrini. Distributed and overlapping representations of faces and objects in ventral temporal cortex. *Science*, 293(5539):2425–2430, 2001. 1
- [9] T. Horikawa and Y. Kamitani. Generic decoding of seen and imagined objects using hierarchical visual features. *Nature communications*, 8:15037, 2017. 10
- [10] Z. Jiao, X. Gao, Y. Wang, J. Li, and H. Xu. Deep convolutional neural networks for mental load classification based on eeg data. *Pattern Recognition*, 76:582–595, 2018. 1
- [11] Y. Kamitani and F. Tong. Decoding the visual and subjective contents of the human brain. *Nature neuroscience*, 8(5):679, 2005. 1
- [12] K. N. Kay, T. Naselaris, R. J. Prenger, and J. L. Gallant. Identifying natural images from human brain activity. *Nature*, 452(7185):352, 2008. 1
- [13] N. Kriegeskorte. Deep neural networks: a new framework for modeling biological vision and brain information processing. *Annual review of vision science*, 1:417–446, 2015. 2
- [14] S. Kullback and R. A. Leibler. On information and sufficiency. *The annals of mathematical statistics*, 22(1):79–86, 1951. 3
- [15] A. B. L. Larsen, S. K. Sønderby, H. Larochelle, and O. Winther. Autoencoding beyond pixels using a learned similarity metric. *arXiv preprint arXiv:1512.09300*, 2015. 4
- [16] L. v. d. Maaten and G. Hinton. Visualizing data using t-sne. *Journal of machine learning research*, 9(Nov):2579–2605, 2008. 6
- [17] T. M. Mitchell, S. V. Shinkareva, A. Carlson, K.-M. Chang, V. L. Malave, R. A. Mason, and M. A. Just. Predicting human brain activity associated with the meanings of nouns. *science*, 320(5880):1191–1195, 2008. 1
- [18] Y. Miyawaki, H. Uchida, O. Yamashita, M.-a. Sato, Y. Morito, H. C. Tanabe, N. Sadato, and Y. Kamitani. Visual image reconstruction from human brain activity using a combination of multiscale local image decoders. *Neuron*, 60(5):915–929, 2008. 1, 2, 6
- [19] T. Naselaris, R. J. Prenger, K. N. Kay, M. Oliver, and J. L. Gallant. Bayesian reconstruction of natural images from human brain activity. *Neuron*, 63(6):902–915, 2009. 1
- [20] B. Ng and R. Abugharbieh. Generalized group sparse classifiers with application in fmri brain decoding. In *Computer Vision and Pattern Recognition (CVPR), 2011 IEEE Conference on*, pages 1065–1071. IEEE, 2011. 1
- [21] S. Nishimoto, A. T. Vu, T. Naselaris, Y. Benjamini, B. Yu, and J. L. Gallant. Reconstructing visual experiences from brain activity evoked by natural movies. *Current Biology*, 21(19):1641–1646, 2011. 1
- [22] S. Palazzo, C. Spampinato, I. Kavasidis, D. Giordano, and M. Shah. Generative adversarial networks conditioned by brain signals. *PDF available on ucf.edu*, 2017. 2
- [23] R. A. Poldrack and M. J. Farah. Progress and challenges in probing the human brain. *Nature*, 526(7573):371, 2015. 1
- [24] A. Radford, L. Metz, and S. Chintala. Unsupervised representation learning with deep convolutional generative adversarial networks. *arXiv preprint arXiv:1511.06434*, 2015. 4

- [25] P. R. Roelfsema, D. Denys, and P. C. Klink. Mind reading and writing: the future of neurotechnology. *Trends in cognitive sciences*, 2018. 1
- [26] T. Salimans, I. Goodfellow, W. Zaremba, V. Cheung, A. Radford, and X. Chen. Improved techniques for training gans. In *Advances in Neural Information Processing Systems*, pages 2234–2242, 2016. 4
- [27] S. Schoenmakers, M. Barth, T. Heskes, and M. van Gerven. Linear reconstruction of perceived images from human brain activity. *NeuroImage*, 83:951–961, 2013. 2, 6
- [28] K. Seeliger, U. Güçlü, L. Ambrogioni, Y. Güçlütürk, and M. van Gerven. Generative adversarial networks for reconstructing natural images from brain activity. *NeuroImage*, 181:775–785, 2018. 2
- [29] C. Spampinato, S. Palazzo, I. Kavasidis, D. Giordano, N. Souly, and M. Shah. Deep learning human mind for automated visual classification. In *Proceedings of the IEEE Conference on Computer Vision and Pattern Recognition*, pages 6809–6817, 2017. 1
- [30] B. Thirion, E. Duchesnay, E. Hubbard, J. Dubois, J.-B. Poline, D. Lebihan, and S. Dehaene. Inverse retinotopy: inferring the visual content of images from brain activation patterns. *Neuroimage*, 33(4):1104–1116, 2006. 1
- [31] L. Van der Maaten. A new benchmark dataset for handwritten character recognition. *Tilburg University*, pages 2–5, 2009. 6
- [32] M. A. van Gerven, F. P. de Lange, and T. Heskes. Neural decoding with hierarchical generative models. *Neural computation*, 22(12):3127–3142, 2010. 2, 6
- [33] W. Wang, R. Arora, K. Livescu, and J. Bilmes. On deep multi-view representation learning. In *International Conference on Machine Learning*, pages 1083–1092, 2015. 2
- [34] Z. Wang, A. C. Bovik, H. R. Sheikh, and E. P. Simoncelli. Image quality assessment: from error visibility to structural similarity. *IEEE transactions on image processing*, 13(4):600–612, 2004. 8
- [35] D. L. Yamins and J. J. DiCarlo. Using goal-driven deep learning models to understand sensory cortex. *Nature neuroscience*, 19(3):356, 2016. 2